J Appl Electrochem (2012) 42:11–20
DOI 10.1007/s10800-011-0365-1

ORIGINAL PAPER

Study of the influence of a boric–sorbitol complex on Zn–Mn electrodeposition and on the morphology, chemical composition, and structure of the deposits

W. Rubin · E. M. de Oliveira · I. A. Carlos

Received: 28 July 2011 / Accepted: 29 October 2011 / Published online: 23 November 2011

Abstract Zn–Mn electrodeposition onto Pt from an electrolyte containing boric–sorbitol complex (BSC) or boric acid alone (BA) was studied. The influence of BA or BSC content on the deposition process was investigated by cyclic voltammetry and electrodeposits, produced potentiostatically, were analysed by SEM, EDX, and XRD. The voltammetric studies indicated that an increase in the BSC concentration led to a decrease in the deposition current density. EDX analysis of deposits obtained at −1.60 V showed that increasing the BA or BSC concentration in the bath induced a fall in the Mn content of the electrodeposit and that for BSC this decrease was more significant. SEM images showed that the Zn–Mn electrodeposit obtained in the presence of 0.24 M BSC were smoother than other deposits; hence, BSC acted as a grain refiner at this concentration. XRD analysis of this deposit indicated that it was composed of Zn, Mn, $MnZn_{13}$, and $MnH_{0.8}$.

Keywords Zn–Mn · Electrodeposition · Boric acid · Boric–sorbitol complex · X-ray diffraction

1 Introduction

Numerous features of Zn alloys make them very attractive for industrial applications, especially for steel corrosion protection and also as electrodes for batteries [1–12]. In particular, Zn–Mn alloy is thermodynamically nobler than Zn; hence, coatings of Zn alloys are more durable than pure Zn coatings of the same thickness. Also, Zn–Mn alloys show passivating behavior in a chloride environment [13]. A common failure mode of Zn electrodes in Zn-based batteries arises from dendritic growth during charge/discharge cycles and there have been reports of Zn alloys and/or organic inhibitors being used in batteries to suppress the dendrites and thus reduce the zinc corrosion [14].

Zn–Mn deposition has important drawbacks, particularly in regard to process control and current efficiency [13]. The literature reports that Zn–Mn electrodeposits are produced mainly from solutions of citrate-sulphate [1–8, 15–20] and citrate–EDTA [21–23]. However, the main problem in working with these baths is the precipitation of a manganese–citrate complex, leading to an unstable solution and low current efficiency [2, 3]. Baths containing ammonium salts favor Mn deposition, but they tend to be avoided nowadays, since their by-products ammonia and nitrite can be extremely toxic [2]. Fluoroborate [8] and chloride [24–26] baths must also be avoided because of their toxicity and corrosiveness. Hence, it would be interesting to develop alternative Zn–Mn electrodeposition baths, with non-toxic additive, that are less aggressive than these and do not lead to solution instability or highly toxic products.

Accordingly, our laboratory has made a study of polyalcohols as additives in acid or alkaline plating baths and these compounds have been shown to make deposits brighter and more even. In general, the electrodeposited films are free of cracks and dendrites [27–39]. Also, polyalcohols in the alkaline plating bath inhibit the corrosion of zinc [28, 39]. Moreover, we have observed in these experiments that when boric acid and sorbitol are both added to the Zn deposition bath, forming a boric–sorbitol complex (BSC), its pH does not shift over several voltammetric deposition cycles [38], differently from baths without or with boric acid (BA) alone or with BA and

W. Rubin · E. M. de Oliveira · I. A. Carlos (✉)
Departamento de Química, Universidade Federal de São Carlos, CP 676, São Carlos, SP CEP 13565-905, Brazil
e-mail: diac@ufscar.br

glycerol. Therefore, in this study, we developed a Zn–Mn deposition bath containing BSC. Voltammetry was used to investigate the deposition process. SEM, EDS, and XRD analyses of the Zn–Mn deposits were performed to determine their morphology, composition, and phase composition, respectively.

2 Experimental

All chemicals were of analytical grade. Distilled deionized water was used throughout. Zn–Mn electrodeposits were produced in baths containing 0.14 mol L^{-1} $MnSO_4$ + 0.10 mol L^{-1} $ZnSO_4$, with 0.0, 0.080, or 0.24 mol L^{-1} of BA or BSC (Table 1). The five different Zn–Mn baths were denominated A, B, C, D, and E, as shown in the table. We have reported [38] that sorbitol reacts with boric acid, resulting in a complex of two molecules of sorbitol per borate ion: ($2\,C_6H_{14}O_6 + H_3BO_3 \leftrightarrow H^+[C_{12}H_{24}O_{12}B]^- + 3H_2O$). Hence, to form BSC at 0.080 or 0.24 mol L^{-1}, BA and sorbitol were added to the bath in the molar proportion 1:2 (Table 1). The pH of the freshly prepared deposition baths A (without additives), B (0.080 mol L^{-1} BA), C (0.080 mol L^{-1} BSC), D (0.24 mol L^{-1} BA) and E (0.24 mol L^{-1} BSC) were, respectively, 3.50, 3.65, 3.40, 3.65, and 2.95. Thus, the pH of baths A, C, and E had to be adjusted to ~3.65 with NaOH. It must be stressed that the baths without any additive or with BA alone were studied in comparison with those containing BSC to investigate the influence of the complex boric-sorbitol formed. After various voltammetric cycles, the pH of the baths containing BSC did not shift, while those containing BA alone or no additives had to be readjusted to 3.65, with NaOH.

At this pH, BA is in the undissociated form ($K_a = 6.4 \times 10^{-10}$) [40]. When a polyalcohol is added to a solution containing BA, it behaves as a stronger acid. For example, the K_a of the boric–mannitol complex is $\sim 1.5 \times 10^{-4}$, and the K_a of BSC would probably be of the same order of magnitude since mannitol is an isomer of sorbitol [41].

Each electrochemical experiment was performed in a freshly prepared acid bath. A Pt disk (0.196 cm^2), a Pt plate and an $Hg/Hg_2Cl_2/KCl$ (0.10 mol L^{-1}) system were employed as working, auxiliary and reference electrodes, respectively. Immediately prior to the electrochemical measurements, the Pt working electrode was polished with 0.3 μm alumina powder, dipped in a concentrated sulphuric-nitric acid mixture and then rinsed with double-distilled water. Potentiodynamic curves were recorded with a GAMRY PCI-4 750 mA potentiostat/galvanostat, at a sweep rate of 10 mV s^{-1}. All experiments were carried out at room temperature (25 °C). Potentiostatic deposits were formed at −1.50 V or −1.60 V, with a deposition charge density (q_d) of 10.20 C cm^{-2}. The deposition current efficiency (CE) was calculated from the stripping/deposition charge ratio [28, 29, 36–38]. In these experiments, Zn–Mn deposits were formed with $q_d = 10.20$ C cm^{-2}. Preliminary tests were conducted to choose the conditions in which to dissolve the electrodeposits. Initially, the dissolution was carried out in 0.10 mol L^{-1} HNO_3 at a sweep rate of 10 mV s^{-1}. However, hydrogen bubbles were seen to form during this process, owing to chemical dissolution of the metal in the acid; at 0.030 mol L^{-1} HNO_3, there was no formation of hydrogen bubbles, and the CE was greater. Thus, nitric acid at 0.030 mol L^{-1} was chosen for Zn–Mn electrodeposit dissolution. The CE was calculated as the mean result in triplicate tests and the experimental error was 2%. Scanning electron microscope with field emission gun (SEM-FEG) photographs were taken with a Philips XL 30 microscope. EDS measurements were made with an eLX Oxford microscope, equipped with EDS Si/Li with an ultra-thin Be window. XRD patterns were produced with Cu Kα radiation (1.5406 Å), using a Rigaku Rotaflex RU200B X-ray goniometer, in 2θ scanning mode (fixed $\omega = 2^\circ$).

Table 1 Composition of the deposition baths (mol L^{-1})

Baths	$ZnSO_4$	$MnSO_4$	H_3BO_3	Sorbitol
A	0.10	0.14	–	–
B	0.10	0.14	0.080	–
C	0.10	0.14	0.080	0.16
D	0.10	0.14	0.24	–
E	0.10	0.14	0.24	0.48

3 Results and discussion

3.1 Electrodeposition of Zn–Mn

First, in order to investigate Zn and Mn electrodeposition separately, voltammograms were recorded on a Pt substrate in deposition baths containing only the Mn salt or the Zn salt, together with the additive BA or BSC, at two different concentrations.

Analyzing the Mn reduction process (Fig. 1) in the negative-going sweep, with BA (—) or BSC (—), at (a) 0.080 mol L^{-1} or (b) 0.24 mol L^{-1}, in the deposition bath, a cathodic peak, and a cathodic wave were seen, while beyond these, cathodic current density (j_c) increased significantly, due to the HER in parallel to Mn reduction. In the presence of BSC (—), the HER was shifted ~0.30 V in the positive direction. It must be pointed out that the reduction of Mn, with BA (—) or BSC (—), at either 0.080 or 0.24 mol L^{-1}, present in the deposition bath, was

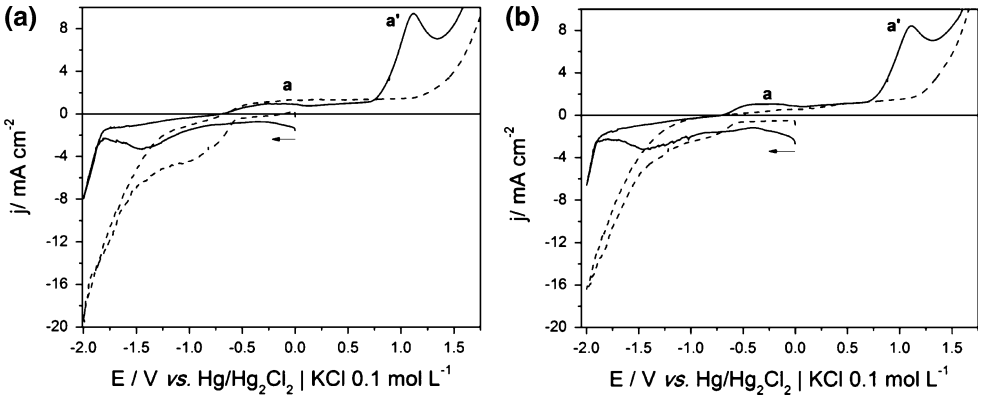

Fig. 1 Voltammetric curves for Pt substrate in 0.14 mol L^{-1} $MnSO_4$ with BA (—) or BSC (– – –) at two different concentrations: (**a**) 0.080 mol L^{-1} and (**b**) 0.24 mol L^{-1}

monitored by visual inspection of the electrode at various reversal potentials terminating the cathodic sweep, and that Mn film was only seen on the electrode at ~ -1.55 V, with 0.080 mol L^{-1} BA or BSC. Sylla et al. [42] reported that they could not see the exact potential at which Mn deposition starts, since the HER occurred in parallel to Mn deposition.

The anodic branches of the voltammetric curves (Fig. 1a, b) show a wave, a ($E = \sim -0.20$ V), and a peak, a' ($E = \sim +1.10$ V), which correspond to the formation of manganese oxides. Pourbaix [43] shows that formation of manganese oxide is possible under these conditions of pH and potential. To investigate further the formation of manganese oxide, positive-going voltammetric curves of Pt in manganese solution were generated, in the presence of BA or BSC, as shown in Fig. 2. It can be seen that the anodic curves formed in Mn solution with BA, at either concentration ((Fig. 2 (—) and (···)), clearly showed anodic current from $\sim +0.10$ V and a peak a' at $\sim +1.10$ V, while with BSC, again at either concentration, the peak a' was suppressed (Fig. 2 (– – –), (-·-·-)). These results indicate that BSC inhibited manganese oxide formation.

In order to determine the anodic processes corresponding to solutions of the additives alone, anodic voltammetric curves for Pt in solutions containing only BA or BSC were performed, at both concentrations, as shown in Fig. 3. It can be seen that the only anodic process observed was the oxidation of BSC, located between ~ -0.60 V and $+0.50$ V and visible only in the solution of 0.24 mol L^{-1} BSC (Fig. 3(-·-·-)).

These results imply not only that the dissolution of the manganese deposit, formed in the cathodic scan at -1.55 V, leads to manganese oxide formation (Fig. 1) but also that this oxide can be formed directly from Mn solution, as seen in Fig. 2.

Figure 4a, b shows the Zn deposition voltammograms recorded from baths containing BA (—) or BSC (– – –), at 0.080 and 0.24 mol L^{-1}, respectively. It can be seen that the zinc deposition was characterized by a cathodic wave

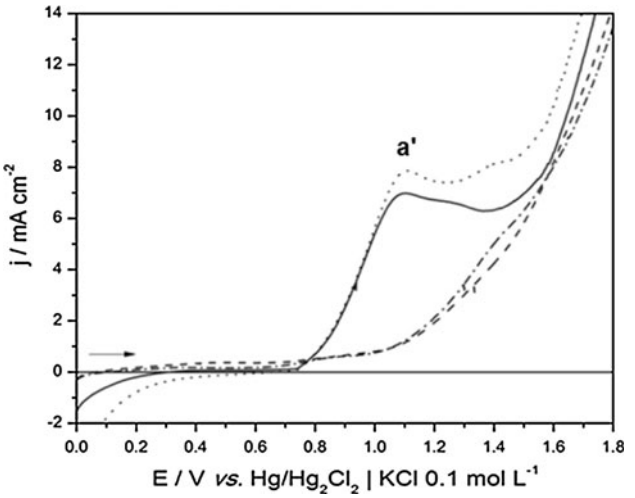

Fig. 2 Anodic voltammetric curves for Pt substrate in 0.14 mol L^{-1} $MnSO_4$ with: (—) 0.080 mol L^{-1} BA, (···) 0.24 mol L^{-1} BA, (– –) 0.080 mol L^{-1} BSC, (-·-) 0.24 mol L^{-1} BSC

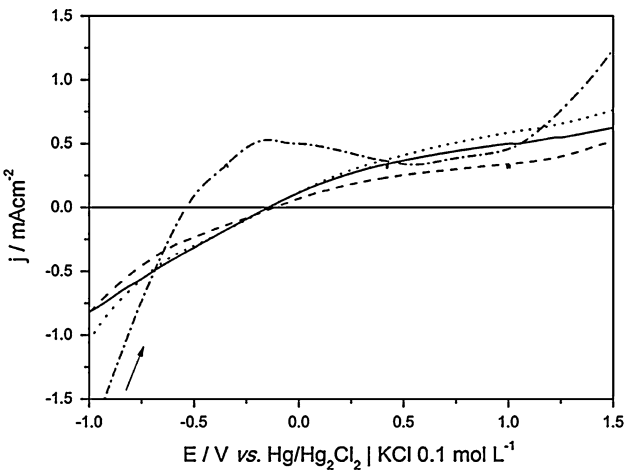

Fig. 3 Anodic voltammetric curves for Pt substrate in 0.080 mol L^{-1} BA (—); 0.080 mol L^{-1} BSC (– – –); 0.24 mol L^{-1} BA (···); 0.24 mol L^{-1} BSC (-·-)

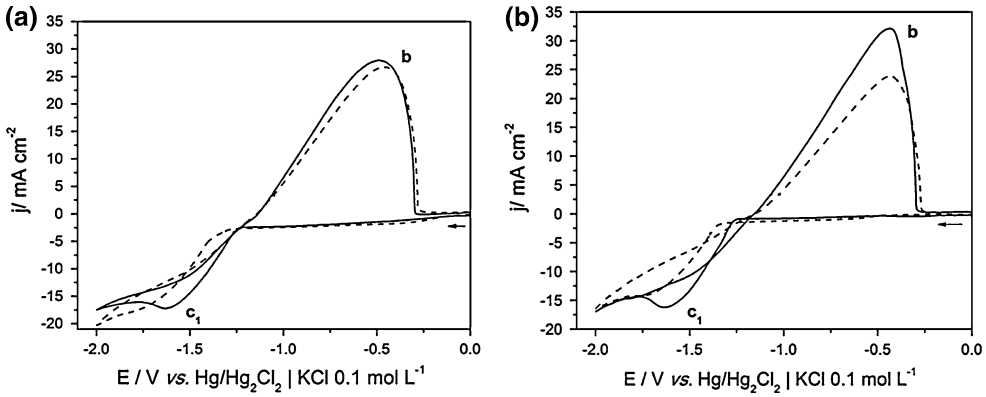

Fig. 4 Voltammetric curves for Pt substrate in 0.10 mol L^{-1} $ZnSO_4$ with BA (—) or BSC (– – –), at two different concentrations: (**a**) 0.080 mol L^{-1} and (**b**) 0.24 mol L^{-1}

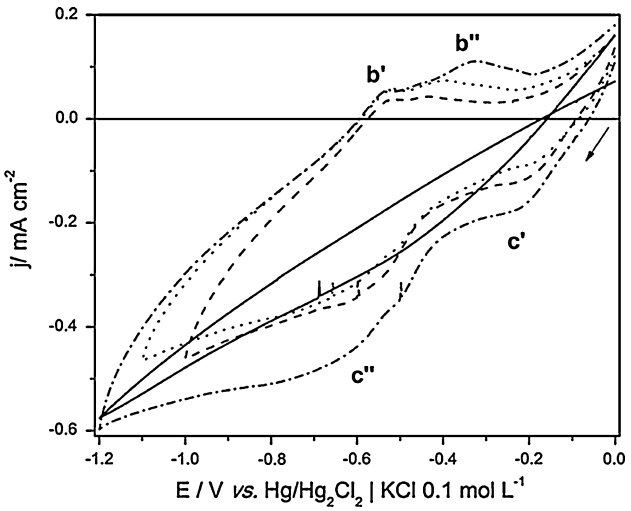

Fig. 5 Voltammetric curves for Pt substrate in 0.24 mol L^{-1} BA (—) or in 0.10 mol L^{-1} $ZnSO_4$ + 0.24 mol L^{-1} BA, pH = 3.65, with various limit potentials: −1.0 V (– – –), −1.1 V (···) and −1.2 V (–·–)

between 0 and −1.10 V and a cathodic peak c_1. In the return (positive-going) sweep, there is an anodic peak b (Fig. 4a, b) at ∼−0.50 V. Figure 4b shows that an increase in the BA or BSC concentration shifted the initial deposition potential (E_d) to more negative values, viz. from −1.22 to −1.25 V and −1.28 to −1.32 V, respectively, while increasing the BSC concentration also led to a reduction in the j_c.

The analysis of the Zn deposition, in the initial moments of the potentiodynamic sweep, became clearer when the sweep was reversed at various limit potentials (Fig. 5). Voltammetric curves of a Pt electrode in a solution containing 0.10 mol L^{-1} $ZnSO_4$ + 0.24 mol L^{-1} BA show two waves in the negative sweep: c' (∼62 μC cm^{-2}) and c'' (∼225 μC cm^{-2}), the first due to the adsorption of species present in the deposition bath and the second to the HER occurring in parallel to Zn reduction. In the positive-going process, there are two peaks, b' and b''. The area under peak b'' increases as the negative-going sweep limit potential becomes more negative, since the amount of metal deposited increases at more negative potentials, whereas that of b' remains approximately constant. It must be stressed that in the region of peak c', no hydrogen bubbles were seen by naked eye. However, in the region of peak c'', HER was seen. The consequent rise in pH at the metal/solution interface would lead to an alkaline layer. Thus, in the initial moments of Zn deposit dissolution, i.e., ∼ −0.57 V, zinc hydroxide was precipitated, leading to the formation of peak b' and, after this, dissolution of the zinc film deposited led to another peak (b''). For comparison, cyclic voltammetry of the Pt electrode was carried out in a solution containing 0.24 mol L^{-1} BA alone (Fig. 5(—)). It can be seen that the HER begins at ∼−0.30 V and that no anodic process occurs in the region of peaks b' and b''. Similar results were obtained with BSC in the deposition bath.

It is reported [39, 44] that zinc deposition starts with primary nucleation and growth of zinc, which is followed by secondary nucleation and growth. Thus, in this study, primary nucleation and growth of zinc occurred at −1.00 V, while secondary nucleation and growth occurred at potentials more negative than ∼−1.20 V.

Figure 6 shows the main features of the Zn–Mn deposition voltammograms, without additives (—) and with BA (– – –) or BSC (···), both at the two concentrations, (a) 0.080 or (b) 0.24 mol L^{-1}. It can be seen that the negative-going voltammetric curves were similar except that increasing the BSC concentration (Fig. 6b (···)) led to a fall in j_c, as in zinc deposition (Fig. 4b (– – –)). It is reported that this reduction in the current density may represent an inhibition of deposition and/or a reduction in the active area of the electrodeposits [30]. The relevance of these results is that the presence of 0.24 mol L^{-1} BSC in the deposition bath may lead to a better quality deposit than those formed in the other baths. Moreover, it can be seen that at this higher concentration of BSC, the deposition potential was shifted to more negative values, suggesting that BSC had been

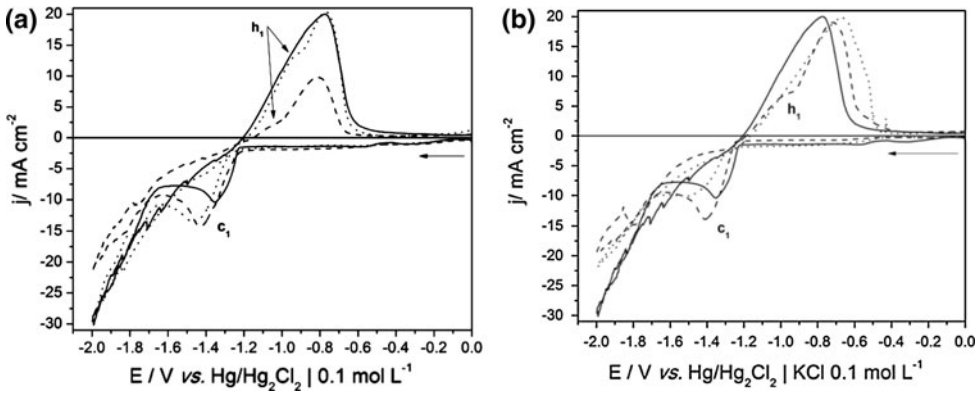

Fig. 6 Voltammetric curves for Pt substrate in 0.10 mol L^{-1} $ZnSO_4$ + 0.14 mol L^{-1} $MnSO_4$ without additives (—) or with BA (– – –) or BSC (···) at two different concentrations of the additive: (**a**) 0.080 mol L^{-1} or (**b**) 0.24 mol L^{-1}

adsorbed on the Pt substrate. These results corroborate those in the literature [38].

It can be seen that the Mn reduction at ~ -1.55 V (Fig. 1) is at a potential close to that of bulk zinc deposition at ~ -1.40 V (Fig. 4). In addition, as will be seen in Sect. 3.2.1, Zn–Mn codeposition occurred at -1.50 V. Moreover, comparing Figs. 1 and 4, the zinc deposition current density is higher than that for manganese deposition, suggesting that Zn–Mn deposits richer in zinc should be obtained in the presence of BA or BSC. The Zn–Mn deposits obtained voltammetrically were analyzed by EDS (see Sect. 3.2.1).

Anodic voltammetric curves (Fig. 6a, b) show only one anodic peak in the absence of the additives. However, with BA or BSC in the bath, a shoulder (h_1) appears in addition to the anodic peak. These results indicate that both BA and BSC led to Zn–Mn dissolution/passivation (shoulder h_1) and then Zn–Mn deposit dissolution, leading to another rise and fall in current density (peak), due to the disappearance of the deposit.

The current efficiency (CE) of Zn–Mn deposition was calculated from the stripping/deposition charge density ratio (Table 2). The Zn–Mn eletrodeposits obtained at -1.60 V and a deposition charge density (q_d) of 10.20 C cm^{-2} were stripped voltammetrically in 0.030 mol L^{-1} HNO_3. The CE values were well below 100%, denoting hydrogen discharge in parallel with the deposition process. In addition, the presence of compounds containing oxygen (see Sect. 3.2.2) in the deposits lowered the CE further. The CE value achieved in the presence of 0.24 mol L^{-1} BSC was the highest, at approximately 50%. In this case, the deposit contained the highest Zn content (92.76 wt%) and the lowest oxygen content (7.24 wt%) among all deposits (see Sect. 3.2.2). The lowest CE (28%) was observed in the bath with 0.080 mol L^{-1} BA. The O and Zn contents in this deposit were the highest and the lowest, respectively; hence the low CE value.

It can be inferred from these results that the presence of BSC in the deposition bath contributed, more significantly than BA, to high CE values.

Table 2 Zn–Mn deposition current efficiency (CE) at -1.60 V in five different deposition baths containing 0.10 mol L^{-1} $ZnSO_4$ +0.14 mol L^{-1} $MnSO_4$ with additives: (A) none; (B) 0.080 mol L^{-1} BA; (C) 0.080 mol L^{-1} BSC; (D) 0.24 mol L^{-1} BA; (E) 0.24 mol L^{-1} BSC

Bath	Current efficiency (%)
A	34.6
B	28.9
C	38.0
D	37.4
E	47.0

3.2 Characterization of Zn–Mn electrodeposits

3.2.1 EDS analysis of electrodeposits obtained voltammetrically

In order to confirm the propositions deduced from the voltammetric curves (Sect. 3.1) for Zn and Mn co-deposition, voltammetric electrodeposits formed under the same conditions as in the deposition baths were analyzed by EDS (Table 3).

It is important to emphasize that in the Zn–Mn voltammetric electrodeposition experiments, the reversal potential was at -1.60 V and that the electrodeposition

Table 3 EDS analysis of Zn–Mn electrodeposits produced by voltammetry in plating baths containing 0.10 mol L^{-1} $ZnSO_4$ + 0.14 - mol L^{-1} $MnSO_4$ plus: (A) no additive; (B) 0.080 mol L^{-1} BA; (C) 0.080 mol L^{-1} BSC; (D) 0.24 mol L^{-1} BA; (E) 0.24 mol L^{-1} BSC

Bath	q_d/C cm^{-2}	Element contents (wt%)		
		Zn	Mn	O
A	0.86	43.74	3.10	53.16
B	0.63	100.00	–	–
C	1.74	39.61	1.91	58.48
D	1.18	47.32	1.10	51.58
E	1.58	16.61	4.43	78.96

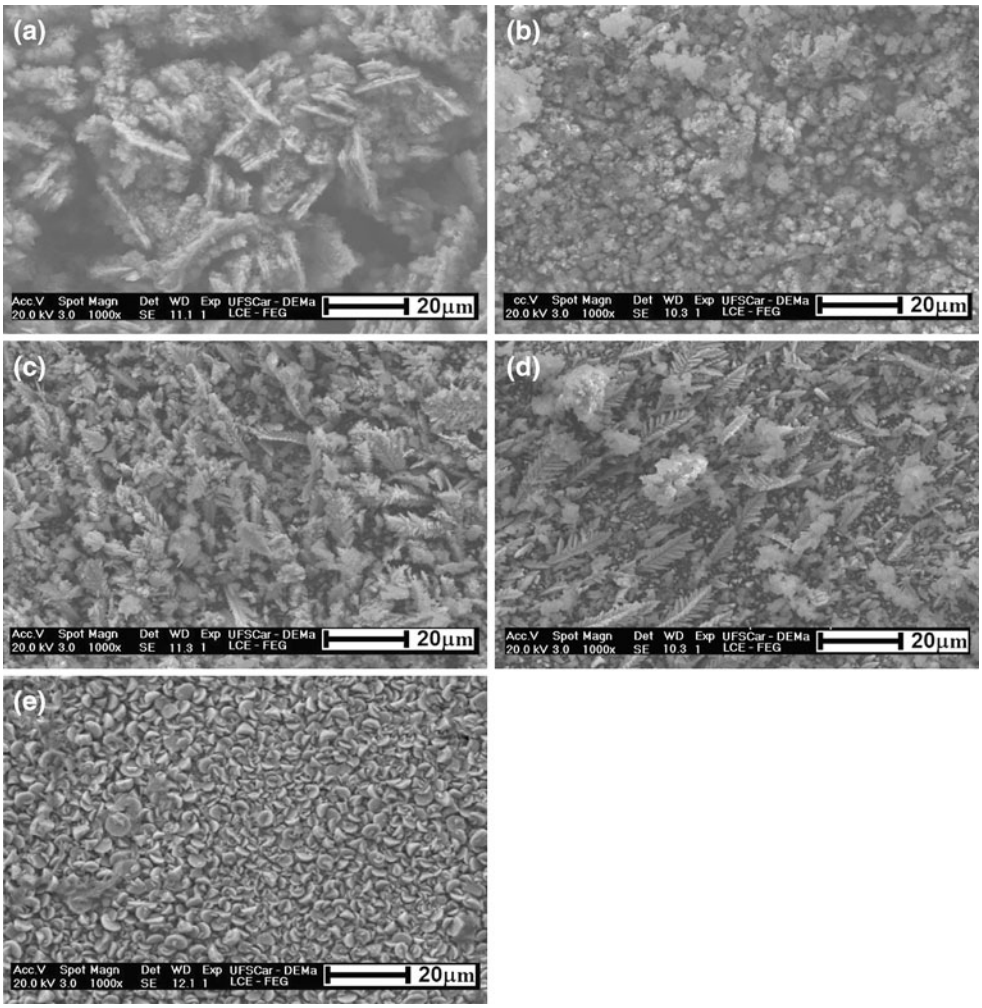

Fig. 7 SEM micrographs of Zn–Mn electrodeposits of charge density 10.20 C cm^{-2} produced potentiostatically from −0.10 V to −1.60 V. Deposition baths containing 0.10 mol L^{-1} $ZnSO_4$ + 0.14 mol L^{-1} $MnSO_4$ with: (**a**) no additive; (**b**) 0.080 mol L^{-1} BA; **c** 0.080 mol L^{-1} BSC; (**d**) 0.24 mol L^{-1} BA; (**e**) 0.24 mol L^{-1} BSC

continued until current density returned to zero. This resulted in electrodeposits with varying deposition charge densities, all of which were 5–16 times lower than those deposits obtained potentiostatically (at −1.60, q_d = 10.20 C cm^{-2}), as will be seen in Sect. 3.2.2.

Table 3 shows that, in general, the electrodeposits contained both Zn and a small amount of Mn, except for the one formed in bath B, with 0.080 mol L^{-1} BA, where, given the low q_d (630 mC cm^{-2}), the Mn content was probably below the detection limit of the technique. These results confirmed the proposed voltammetric co-deposition of Zn and Mn (Sect. 3.1).

3.2.2 SEM and EDS analysis of electrodeposits obtained potentiostatically at −1.60 V

SEM photographs were taken of deposits formed potentiostatically in deposition baths A–E (Table 1) at −1.60 V and a q_d of 10.20 C cm^{-2} (Fig. 7a–e). The deposit produced without any additive was composed of plate sandwich crystallites, distributed irregularly on the surface (Fig. 7a). However, the Zn–Mn deposits obtained in the presence of 0.080 mol L^{-1} BSC (Fig. 7c) or 0.24 mol L^{-1} BA (Fig. 7d) were dendritic, while those obtained in the presence of 0.080 mol L^{-1} BA (Fig. 7b) or 0.24 mol L^{-1} BSC (Fig. 7e) were formed of irregular crystallites or coalesced round plates, respectively. The last deposit (Fig. 7e) was more compact than the others. This deposit, produced in the presence of 0.24 mol L^{-1} (Fig. 7e), was light gray, whereas the remaining were gray. These observations were consistent with the morphology of these deposits.

Table 4 shows the results of the EDS analysis of the electrodeposits shown in Fig. 7. In the absence of additives, the Mn content was 13.67 wt%, rising slightly with 0.080 mol L^{-1} BA in the bath. In deposits produced in the

Table 4 EDS analysis of Zn–Mn electrodeposits of $q_d = 10.2$ C cm^{-2} produced potentiostatically at $E_d = -1.60$ V in plating baths containing 0.10 mol L^{-1} $ZnSO_4$ + 0.14 mol L^{-1} $MnSO_4$ plus: (A) no additive; (B) 0.080 mol L^{-1} BA; (C) 0.080 mol L^{-1} BSC; (D) 0.24 mol L^{-1} BA; (E) 0.24 mol L^{-1} BSC

Bath	Element contents (wt%)		
	Zn	Mn	O
A	74.03	13.67	12.30
B	54.74	15.85	29.41
C	90.73	1.43	7.84
D	81.15	3.07	15.78
E	92.76	0	7.24

Table 5 EDS analysis of Zn–Mn electrodeposits of $q_d = 10.2$ C cm^{-2} produced potentiostatically at $E_d = -1.50$ V in plating baths containing 0.10 mol L^{-1} $ZnSO_4$ + 0.14 mol L^{-1} $MnSO_4$ plus: (A) no additive; (B) 0.080 mol L^{-1} BA; (C) 0.080 mol L^{-1} BSC; (D) 0.24 mol L^{-1} BA; (E) 0.24 mol L^{-1} BSC

Bath	Element contents (wt%)		
	Zn	Mn	O
A	83.02	1.72	15.26
B	85.46	0.77	13.77
C	77.21	–	22.78
D	85.30	1.33	13.37
E	75.82	0.42	23.76

bath with higher BA content, the Mn content decreased dramatically, from 15.85 wt% (0.080 mol L^{-1}) to 3.07 wt% Mn (0.24 mol L^{-1}). In the Zn–Mn deposits produced in the presence of 0.080 mol L^{-1} BSC, the Mn content was only 1.43 wt%, while for 0.24 mol L^{-1} BSC, Mn fell below the detection limit of EDS (see Sect. 3.3, where XRD analysis showed Mn in the deposits). The results obtained here indicate that the BSC inhibited the co-deposition of Mn with Zn and that, depending on the BSC concentration, Mn deposition can be significantly inhibited.

Moreover, in the presence of the higher concentration of BSC, the oxygen content in the deposit was the lowest (7.24 wt%) of the five deposits (Table 4). Sylla et al. [42] showed that adding PEG to the bath decreased the Mn content, but increased the oxygen content in the electrodeposit.

The presence of O in the deposits indicated that, probably, zinc hydroxide, and/or manganese hydroxide had formed, or some dehydration product, such as ZnO and/or MnO, which would need a strong pH rise at the electrode surface, to reach values around 5.0 or 7.5, respectively, at which insoluble $Zn(OH)_2$ and $Mn(OH)_2$ precipitate [43].

Thus, the results of Table 4 indicate that 0.24 mol L^{-1} BSC works better as a buffer than BSC and BA at other concentrations, since the lowest O content in the deposit was obtained in this condition.

3.2.3 *SEM and EDS analysis of electrodeposits obtained potentiostatically at −1.50 V*

In order to check whether Mn is co-deposited with Zn already at −1.50 V, electrodeposits produced at this potential with q_d = 10.20 C cm^{-2} were analyzed by EDS (Table 5). The same electrodeposits were analyzed morphologically by SEM (Fig. 8).

EDS analyses of these electrodeposits (Table 5) showed that the highest Mn content was 1.72 wt%, observed in the deposits produced in the bath (A) without additives. Comparing the EDS analyses of the electrodeposits obtained potentiostatically at −1.60 V (Table 4) and −1.50 V (Table 5), it can be seen that in the latter, the incorporation of oxygen decreased significantly when BA was present in the deposition bath (B and D). Also, in baths containing BSC, at either concentration (C and E), the Zn contents in the electrodeposits obtained at −1.50 V were lower, while the oxygen content was tripled. It is noteworthy that the Mn content of the electrodeposits obtained in the presence of 0.080 mol L^{-1} BSC may be below the detection limit of EDS. Thus, these results corroborate the suggestion made on the basis of the voltammetric curves of Mn is deposition (Fig. 1) that Mn already deposited at −1.50 V, albeit in smaller amounts.

Figure 8a shows that the deposit produced in the bath with no additives consisted of dendritic triangular plates distributed irregularly on the Pt surface. The Zn-Mn deposits produced in the presence of 0.080 mol L^{-1} BA (Fig. 8b) was similar, but composed, in general, of smaller crystallites, while that formed in the presence of 0.24 mol L^{-1} BA (Fig. 8d) consisted of hexagonal plate crystallites, uniformly distributed on the Pt surface. The deposits produced in the presence of 0.080 mol L^{-1} (Fig. 8c) or 0.24 mol L^{-1} BSC (Fig. 8e), were also composed of hexagonal plates, but these deposits were smoother. These results imply that BA, at 0.24 mol L^{-1} (Fig. 8d), and BSC at either concentration (Figs. 8c, e), acted as grain refiners.

SEM analysis shows that Zn–Mn electrodeposits produced with q_d = 10.20 C cm^{-2} at −1.60 V, without additives or with 0.080 mol L^{-1} BA or 0.24 mol L^{-1} BSC, are not dendritic. Further, those produced at −1.50 V with q_d = 10.20 C cm^{-2}, in the presence of 0.24 mol L^{-1} BA or either BSC concentration, are also not dendritic.

3.3 X-ray diffraction analysis of the electrodeposits obtained at −1.60 V

X-ray diffraction was carried out on electrodeposits produced potentiostatically at −1.60 V, with q_d = 10.20 C cm^{-2}. The diffraction patterns were compared with expected values

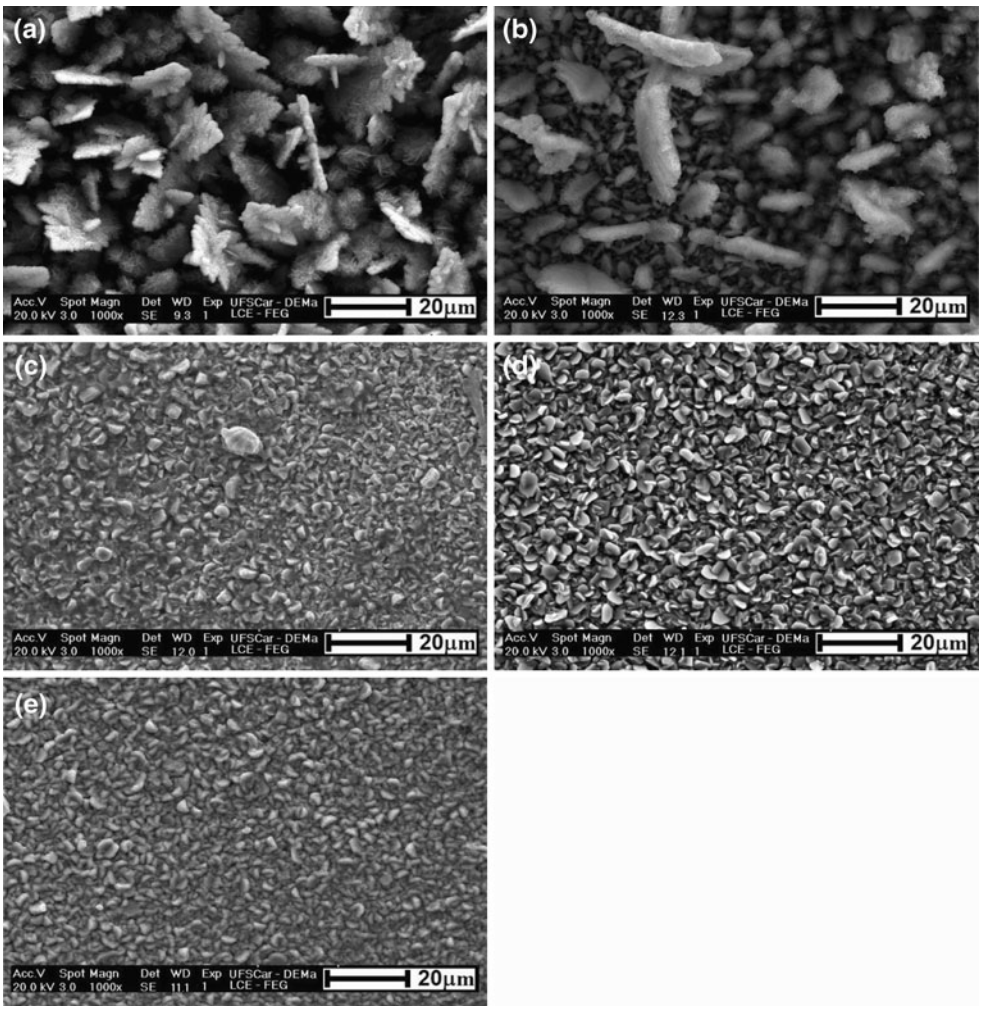

Fig. 8 SEM micrographs of Zn–Mn electrodeposits of charge density 10.20 C cm^{-2} produced potentiostatically from −0.10 V to −1.50 V. Deposition baths containing 0.10 mol L^{-1} $ZnSO_4$ + 0.14 mol L^{-1} $MnSO_4$ with: **a** no additive; **b** 0.080 mol L^{-1} BA; **c** 0.080 mol L^{-1} BSC; **d** 0.24 mol L^{-1} BA; **e** 0.24 mol L^{-1} BSC

given in JCPDS [45] and ICSD [46] (only peaks whose relative intensity was above 10% were selected). Fig. 9a–e shows typical diffractograms for the Zn–Mn deposits produced from baths A–E (Table 1).

These diffractograms show that the electrodeposits were composed of various phases and that, depending on the presence or otherwise of the additives, various phase mixtures were observed (Fig. 9).

The electrodeposit produced from bath A, without additives, was a mixture of Zn, Mn, ZnO, and MnO (Fig. 9a). The presence of 0.080 mol L^{-1} BA in bath B led to a deposit that contained Zn, Mn, MnO, and the alloy $MnZn_{13}$ (Fig. 9b). However, the electrodeposit produced from baths C and D, in the presence of 0.080 mol L^{-1} BSC (Fig. 9c) or 0.24 mol L^{-1} BA (Fig. 9d), respectively, contained only a mixture of Zn and MnO (Fig. 9c), whereas when produced with the higher concentration of complex in bath E (Fig. 9e), the electrodeposit was composed of Zn, Mn, $MnZn_{13}$, and $MnH_{0.8}$. EDS analysis of the latter deposit showed that it contained 7.24 wt% O. However, XRD analysis did not show compounds containing O (Fig. 9e), probably because these compounds were not crystalline.

These results show that Zn and Mn co-deposition occurred and in some cases an alloy ($MnZn_{13}$) was formed. They also show that compounds containing oxygen (ZnO and MnO) were formed during the Zn and Mn deposition, because the HER occurred in parallel to this process, leading to alkalinization of the metal/solution interface and formation of these compounds. The presence of oxides, such as MnO, corroborates the low buffer action of 0.080 mol L^{-1} BSC and BA at either concentration.

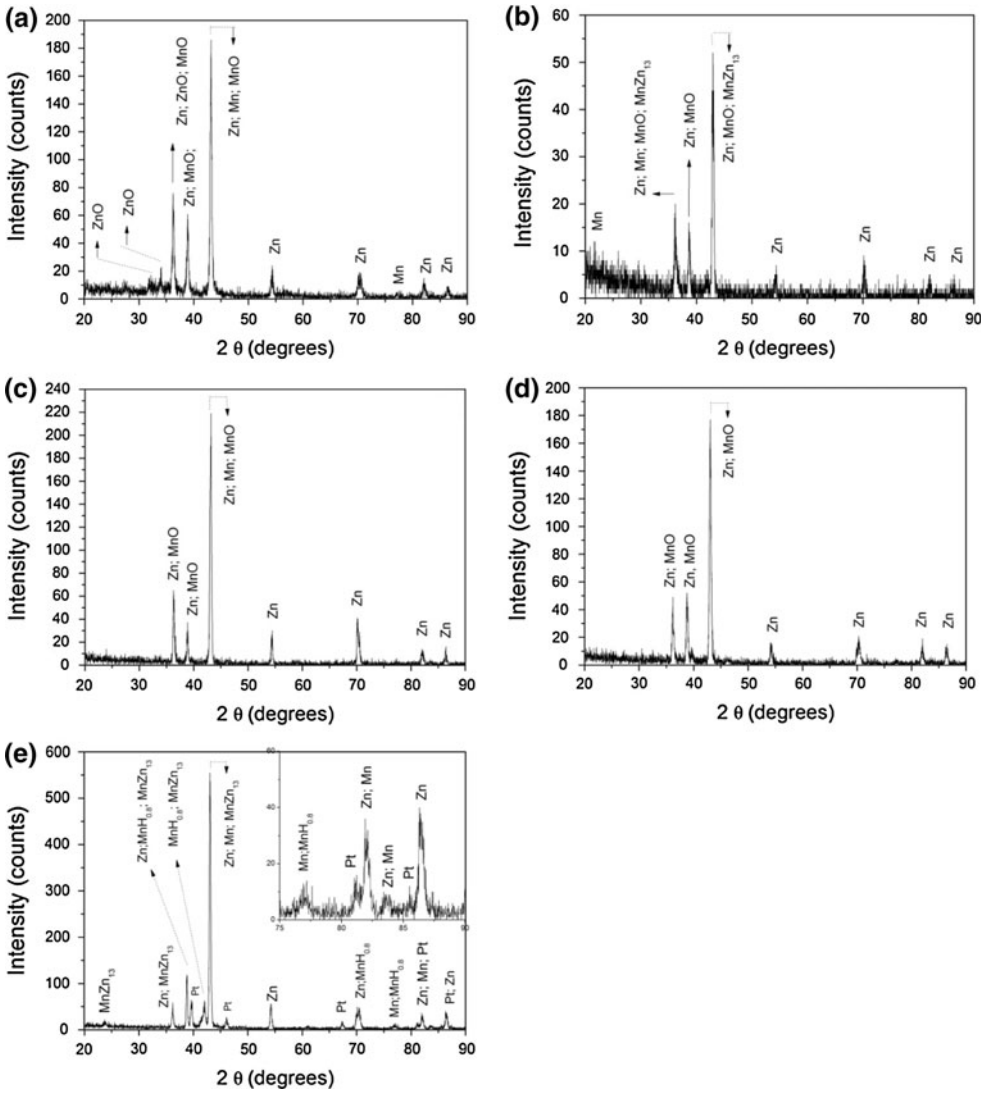

Fig. 9 X-ray diffraction patterns of Zn–Mn electrodeposits of charge density 10.20 C cm^{-2} produced potentiostatically from −0.10 V to −1.60 V, in deposition baths containing 0.10 mol L^{-1} $ZnSO_4$ + 0.14 mol L^{-1} $MnSO_4$ with: **a** no additive; **b** 0.080 mol L^{-1} BA; **c** 0.080 mol L^{-1} BSC; **d** 0.24 mol L^{-1} BA; **e** 0.24 mol L^{-1} BSC

4 Conclusions

Voltammetric studies of Zn–Mn deposition showed that increasing the concentration of the additive BSC led to a decrease in the current density and, when the concentration of either BSC or BA was raised, the deposition potential was shifted to more negative values indicating that adsorption of the additive occurred.

EDS analysis of the electrodeposits produced at −1.50 V, with a charge density of 10.20 C cm^{-2}, indicated that Zn and Mn were already co-deposited at this potential. In the case of the electrodeposits produced at −1.60 V, with the same charge density, it was seen that the presence of BSC in the deposition bath decreased the Mn content in the deposits significantly and, at higher additive concentration, the co-deposition of Mn with Zn was inhibited. BSC also inhibited the formation of compounds containing oxygen more strongly than BA. The formation of these compounds with oxygen, together with the HER occurring in parallel to the metal deposition, lowered the CE to appreciably less than 100%.

SEM analysis of the electrodeposits produced showed that BSC at the higher concentration acted as a grain refiner, since in its presence the electrodeposits were smoother than without it.

XRD analysis indicated that the electrodeposits produced at −1.60 V in the presence of 0.080 mol L^{-1} BA contained the phases Zn, Mn, MnO, and $MnZn_{13}$, whereas those obtained with 0.24 mol L^{-1} BSC were composed of Zn, Mn, $MnZn_{13}$, and $MnH_{0.8}$.

References

1. Lowenheim FA (1974) In: Modern electroplating, 2nd edn. Wiley, New York
2. Brenner A (1963) In: Electrodeposition of alloys principles and practice, vol. 1. Academic Press, New York

3. Gabe DR, Wilcox GD (1993) Corr Sci 35:1251
4. Gabe DR, Wilcox GD, Jamani A, Pearson BR (1993) Met Finish 91:34
5. Wilcox GD, Petersen B (1996) Trans Inst Met Finish 74:15
6. Danilov FI, Sukhomlin DA, Gerasimov VV, Popovich VA (1992) Soviet Electrochem 28:171
7. Srinivasan KN, Selvan M, Venkata KIS (1993) J Appl Electrochem 23:358
8. Sagiyama M, Urakawa T, Adaniya T, Hara T, Fukuda Y (1987) Plat Surf Finish 74:40
9. Boshkov N, Petrov K, Vitkova S, Raichevsky G (2005) Surf Coat Technol 194:276
10. Boshkov N, Petrov K, Kovacheva D, Vitkova S, Nemska S (2005) Electrochim Acta 51:77
11. Boshkov N (2003) Surf Coat Technol 172:217
12. Boshkov N, Petrov K, Raichevsky G (2006) Surf Coat Tech 200:5995
13. Díaz-Arista P, Ortiz ZI, Ruiz H, Ortega R, Meas Y, Trejo G (2009) Surf Coat Tech 203:1167
14. Linden D, Reddy TB (2002) In: Handbook of batteries, 3rd edn. McGraw-Hill, New York
15. Bozzini B, Pavan F, Bollini G, Cavallotti PL (1997) Trans Inst Met Finish 75:175
16. Bozzini B (2000) Trans Inst Met Finish 78:93
17. Bozzini B, Griskonis E, Sulcius A, Cavallotti PL (2001) Plat Surf Finish 88:64
18. Danilov FI, Gerasimov VV, Sukhomlin DA (2001) Russ J Electrochem 37:308
19. Kimpton HJ, Smith CJE, Wilcox GD (2002) Trans Inst Met Finish 80:116
20. Bozzini B, Griskonis E, Fanigliulo A, Sulcius A (2002) Surf Coat Technol 154:294
21. Müller C, Sarret M, Andreu T (2002) J Electrochem Soc 149:C600
22. Müller C, Sarret M, Andreu T (2003) Electrochim Acta 48:2397
23. Müller C, Sarret M, Andreu T (2003) Electrochem Soc 150:C772
24. Sylla D, Savall C, Gadouleau M, Rebere C, Creus J, Refait Ph (2005) J Appl Electrochem 35:1133
25. Savall C, Rebere C, Sylla D, Gadouleau M, Refait Ph, Creus J (2006) Mat Sci Eng A430:165
26. Chen PY, Hussey CL (2007) Electrochim Acta 52:1857
27. Galvani F, Carlos IA (1997) Met Finish 95:70
28. Pereira MS, Barbosa LL, Souza CAC, Moraes ACM, Carlos IA (2006) J Appl Electrochem 36:727
29. Carlos IA, Siqueira JLP, Finazzi GA, Almeida MRH (2003) J P Sour 117:179
30. Carlos IA, Malaquias MA, Oizumi MM, Matsuo TT (2001) J P Sour 92:56
31. Siqueira JLP, Carlos IA (2007) J P Sour 169:361
32. Carlos IA, Oliveira EM, Finazzi G (2004) Surf Coat Tech 187:377
33. Carlos IA, Barbosa LL, Yonashiro M, Carlos RM, Oliveira GM, Almeida MRH (2005) Surf Coat Tech 192:145
34. Carlos IA, Almeida RHH (2004) J Electroanal Chem 562:153
35. Oliveira EM, Finazzi G, Carlos IA (2006) Surf Coat Tech 200:5978
36. Broggi RL, Oliveira GM, Barbosa LL, Pallone EMJA, Carlos IA (2006) J Appl Electrochem 36:403
37. Carlos IA, Barbosa LL (2006) Surf Coat Tech 201:1695
38. Oliveira EM, Carlos IA (2008) J Appl Electrochem 38:1203
39. Carvalho MF, Rubin W, Carlos IA (2010) J Appl Electrochem 40:1625
40. Kotrlý S, Sucha L (1985) In: Handbook of chemical equilibria in analytical chemistry, 3rd edn. Wiley, New York
41. Mendham J, Denne RC, Bassett J, Jeffery GH (1978) In: Vogel's textbook of quantitative inorganic analysis, 4th edn. Longman Inc., London
42. Sylla D, Creus J, Savall C, Roggy O, Gadouleau M, Refait Ph (2003) Thin Solid Films 424:171
43. Pourbaix M (1966) In: Atlas of electrochemical equilibria in aqueous solutions, 2nd edn. Pergamon Press Ltd., Oxford
44. Tulio PC, Carlos IA (2009) J Appl Electrochem 39:283
45. Joint Committee on Powder Diffraction Standards, JCPDS—International Centre for Diffraction Data. Powder Diffraction File-PDF-2 (2000). Database Sets 1–49. ICDD (CD-ROM), Pennsylvania
46. http://icsd.fiz-karlsruhe.de.w10001.dotlib.com.br. Accessed 15 Mar 2011